Received: 7 December 2021 | Revised: 10 June 2022 | Accepted: 20 June 2022

DOI: 10.1002/dvdy.513

RESEARCH ARTICLE

Developmental Dynamics WILEY

Adhesion molecule *Amigo2* is involved in the fasciculation process of the fasciculus retroflexus

Verónica Company | Raquel Murcia-Ramón | Abraham Andreu-Cervera | Paula Aracil-Pastor | Francisca Almagro-García | Salvador Martínez | Diego Echevarría | Eduardo Puelles

Instituto de Neurociencias, Universidad Miguel Hernández de Elche-CSIC, Sant Joan d'Alacant, Alicante, Spain

Correspondence
Eduardo Puelles, Instituto de Neurociencias de Alicante, Universidad Miguel Hernández-CSIC, 03550 San Juan, Alicante, Spain.
Email: epuelles@umh.es

Funding information
Fundación Tatiana Pérez de Guzmán el Bueno, Grant/Award Number: FTPGB18/SM; Generalitat Valenciana, Grant/Award Number: PROMETEO/2018/041; Instituto de Salud Carlos III, Grant/Award Number: RD16/001/0010; Ministerio de Educación, Cultura y Deporte, Grant/Award Number: FPU16/03853; Secretaría de Estado de Investigación, Desarrollo e Innovación, Grant/Award Numbers: BFU2013-48230, SAF2017-83702-R, SEV-2017-0723

Abstract

Background: The fasciculus retroflexus is the prominent efferent pathway from the habenular complex. Medial habenular axons form a core packet whereas lateral habenular axons course in a surrounding shell. Both groups of fibers share the same initial pathway but differ in the final segment of the tract, supposedly regulated by surface molecules. The gene *Amigo2* codes for a membrane adhesion molecule with an immunoglobulin-like domain 2 and is selectively expressed in the medial habenula. We present it as a candidate for controlling the fasciculation behavior of medial habenula axons.

Results: First, we studied the development of the habenular efferents in an *Amigo2* lack of function mouse model. The fasciculus retroflexus showed a variable defasciculation phenotype. Gain of function experiments allowed us to generate a more condensed tract and rescued the *Amigo2* knock-out phenotype. Changes in *Amigo2* function did not alter the course of habenular fibers.

Conclusion: We have demonstrated that *Amigo2* plays a subtle role in the fasciculation of the fasciculus retroflexus.

KEYWORDS

Amigo2, fasciculation, fasciculus retroflexus, lateral habenula, medial habenula

1 | INTRODUCTION

The mammalian central nervous system integrates multiple functional systems. One of them, the limbic system, plays a pivotal role and is related to emotions, behavior, memory and olfaction. This complex system involves neuronal populations located in all cerebral regions: amygdala, hippocampus, cingular cortex, septal, and hypothalamic nuclei in the secondary prosencephalon; thalamic and habenular nuclei in the diencephalon; substantia nigra, ventral tegmental area, periaqueductal gray, and reticular formation in the midbrain; raphe serotoninergic complex, locus coeruleus and reticular formation in the hindbrain.[1] This vast group of different neuronal structures is interconnected by axonal tracts that display stereotyped trajectories Minor alterations in the specification of limbic neuronal subtypes or in their connectivity might account for a variety of syndromes

and pathologies related to the limbic system. These diseases include mental disorders such as substance abuse, schizophrenia and depression, or alterations of normal development that generate disabilities in learning, motivation, reward, pain, and memory mechanisms.[2-7]

The habenular complex is located in the epithalamus (dorsal part of the thalamic progenitor area in alar prosomere 2). It plays a pivotal role in the communication between forebrain components and midbrain and hindbrain neurotransmitter-identified neurons (dopamine, serotonin, etc.). It consists of two major subregions, the medial and the lateral habenular areas (mHb and lHb). Their afferent and efferent fibers are integrated within the so-called "dorsal diencephalic conduction system" (ie, stria medullaris, fasciculus retroflexus).[8,9] Both mHb and lHb project through the fasciculus retroflexus (fr; this is also known as habenulo-interpeduncular tract). The mHb axons aggregate strongly together and occupy the core of the tract, whereas the lHb axons incorporate within the shell of the tract.[10,11] This differential organization of the two components is accompanied by different behavior at their terminal trajectory. The lHb axons defasciculated as they reach the diencephalic basal plate and innervate in a diffuse pattern the meso-diencephalic substantia nigra and the hindbrain raphe formation.[11] In contrast, the mHb axons remain compact as they reach the brain surface next to the diencephalic floor plate and thereafter navigate caudalwards into their selective target, the interpeduncular nucleus located in the ventromedian prepontine hindbrain. Characteristically, these axons sequentially crisscross several times their terminal neuropile from left to right, or vice versa. The developing trajectory of the fr has been described[12] and the related guidance control mechanisms have been partially unveiled.[12-16] These mechanisms require the interaction of the growing axons with long and short distance acting guidance molecules. These processes are accompanied by mutual adhesive interactions between the axons that give rise to the fasciculation of the tracts. These interactions can be homophilic or heterophilic and play a crucial role in the correct generation of the different fascicles.[17-19]

This variant fasciculation behavior of the fr must be due to differential expression of given membrane proteins in the mHb and lHb axonal populations. A particular combination of surface proteins will direct the response of the growing axons to signaling molecules found in their trajectory. The mHb and lHb neurons indeed express differential combinations of axon guidance and cell adhesion molecules, as was demonstrated by laser-capture microdissection and mass spectrometry.[20] Between the molecules enriched in the mHb, Schmidt and collaborators described the presence of well-known proteins such as the *Netrin1* receptor, *Deleted in colon carcinoma* (*DCC*), and also *Neuropilin2* (*Nrp2*), receptor of *Semaphorin3F*. The latter is responsible for the aversive response of mHb fr axons toward the pretectal alar territory.[14,15,21] Other molecules such as *Plexin-B2*[22,23] are not expressed in the habenula in the correct time window when de fr is generated. Interestingly, a leucine-rich-repeat-containing and immunoglobulin-like protein named *amphoterin induced gene and ORF 2*, which is presently known as *adhesion molecule with immunoglobulin like domain 2* (*Amigo2*; Laeremans et al)[24] was detected in the central nervous system. It is especially expressed in the hippocampus.[25-27] *Amigo2* expression in the mHb was described[28] and is confirmed from Allen Institute mouse brain mapping data. It belongs to a family of type I transmembrane proteins that mediates cell-cell interactions by homophilic (Amigo2-Amigo2) and heterophilic (Amigo1-Amigo2-Amigo3) interactions.[26] Such interactions already have been related to neural circuit development[29] and neurite outgrowth and fasciculation.[26]

Various alterations of this gene have been described in humans. Psychomotor development delay detected in two patients with a proximal 12q deletion was related to *Amigo2* loss of function.[30] Genomic analysis of a patient with intellectual disabilities among multiple congenital abnormalities established a direct link to *Amigo2* sequence alterations.[31] Moreover, disfunction of this gene has been described in patients with Occulo-Auriculo-Vertebral Spectrum Disease.[32,33] Finally, overexpression of *Amigo2* has been related to an increment in the metastatic properties of hepatic, lung, gastric, ovarian or melanoma cancers.[34-39]

The specific expression of this marker in the mHb prompted us to select *Amigo2* as a candidate molecule to play a role in the differential final trajectory and/or fasciculation behavior of the mHb vs lHb axons. To examine this hypothesis, we decided to study the effect of *Amigo2* loss and gain of function on murine fr development.

2 | RESULTS

2.1 | Distribution of mHb and lHb axons in the fr

As a first step in our analysis, we checked the differential distribution of fr habenular axons in E15.5mouse brains as they end their dorsoventral course next to the thalamo-pretectal boundary. We labeled the habenular complex by application of a DiI crystal. Corroborating previous data, it was observed that in the vicinity of the substantia nigra pars compacta (SNc; identified by the presence of tyrosine hydroxylase immunoreactivity) the mHb axons remain fasciculated compactly close to the

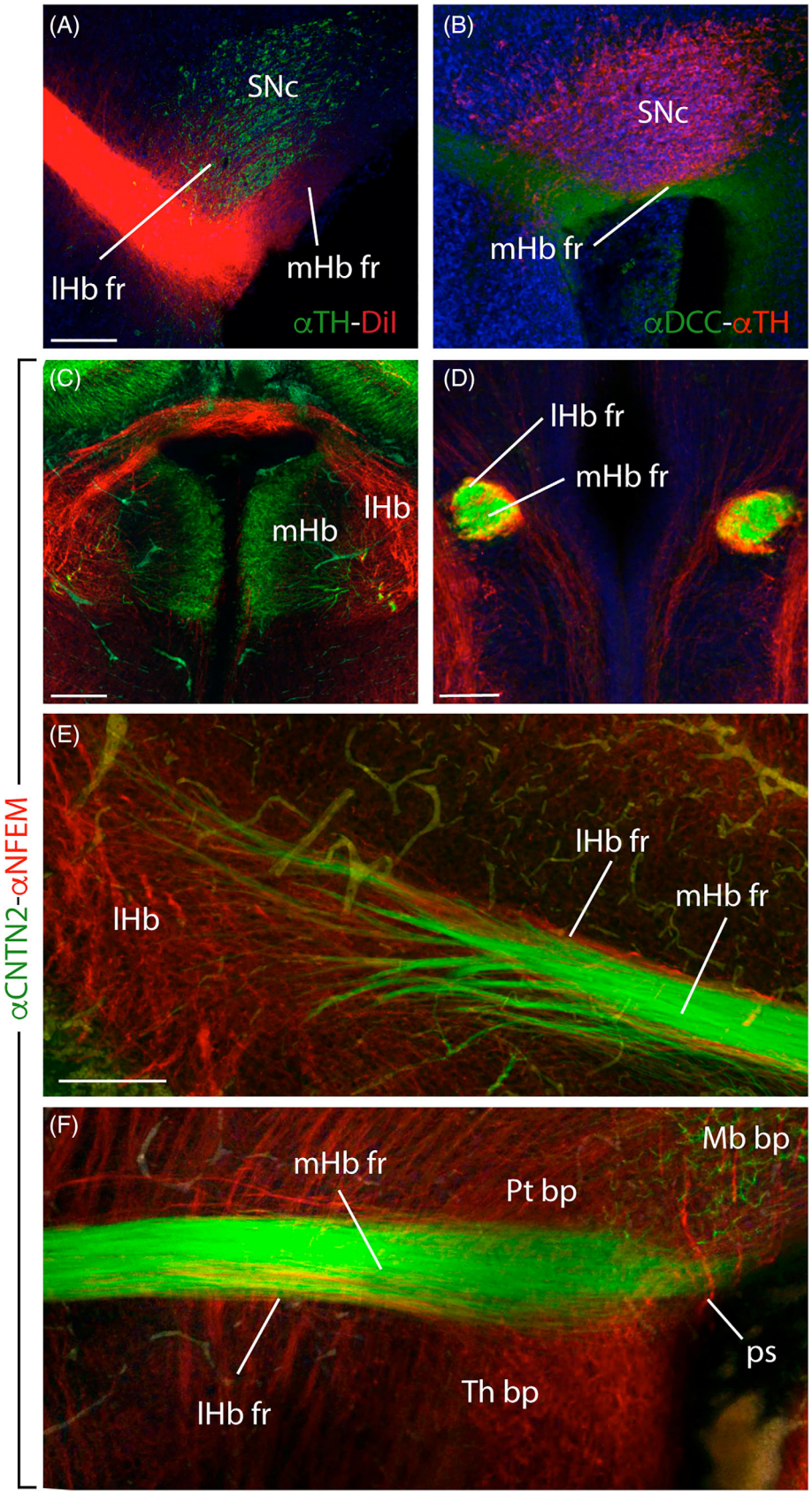

FIGURE 1 Differential behavior between mHb and lHb axons. Sagittal sections (A, B, E, F) and coronal sections (C, D) of E15.5 mouse brains to describe the fr. (A) DiI labeling and αTH immunohistochemistry (IHC). The lHb fr defasciculated and targeted the SNc meanwhile the mHb axons contacted the diencephalic pial surface to travel along the anteroposterior axis along diencephalon, midbrain and finally reach the Ip in r1. (B) αDCC and αTH immunochemistry. DCC specifically labeled the mHb fr axons, which navigate superficially to the SNc. (C-F) α-CNTN2 as a mHb marker and α-NF as a lHb marker by immunochemistry. The distribution of the axons is segregated in the fr depending on their origin, mHb fr axons are placed in the core and lHb fr axons in the sheath of the tract. lHb, lateral habenula; lHb fr, lateral habenular axons of the fasciculus retroflexus, Mb bp, midbrain basal plate; mHb, medial habenula; mHb fr, medial habenular axons of the fasciculus retroflexus; ps, pial surface; Pt bp, pretectal basal plate; SNc, substantia nigra pars compacta; Th bp, thalamic basal plate. Scale bar: 100 μm

pial surface, while the lHb axons defasciculate and innervate the SNc (Figure 1A). The trajectory of mHb axons was confirmed by the presence of DCC, the receptor of *Netrin1* and specific marker of mHb neurons.[20,40] No DCC positive axons defasciculated inside the SNc (Figure 1B). As previously demonstrated, this different

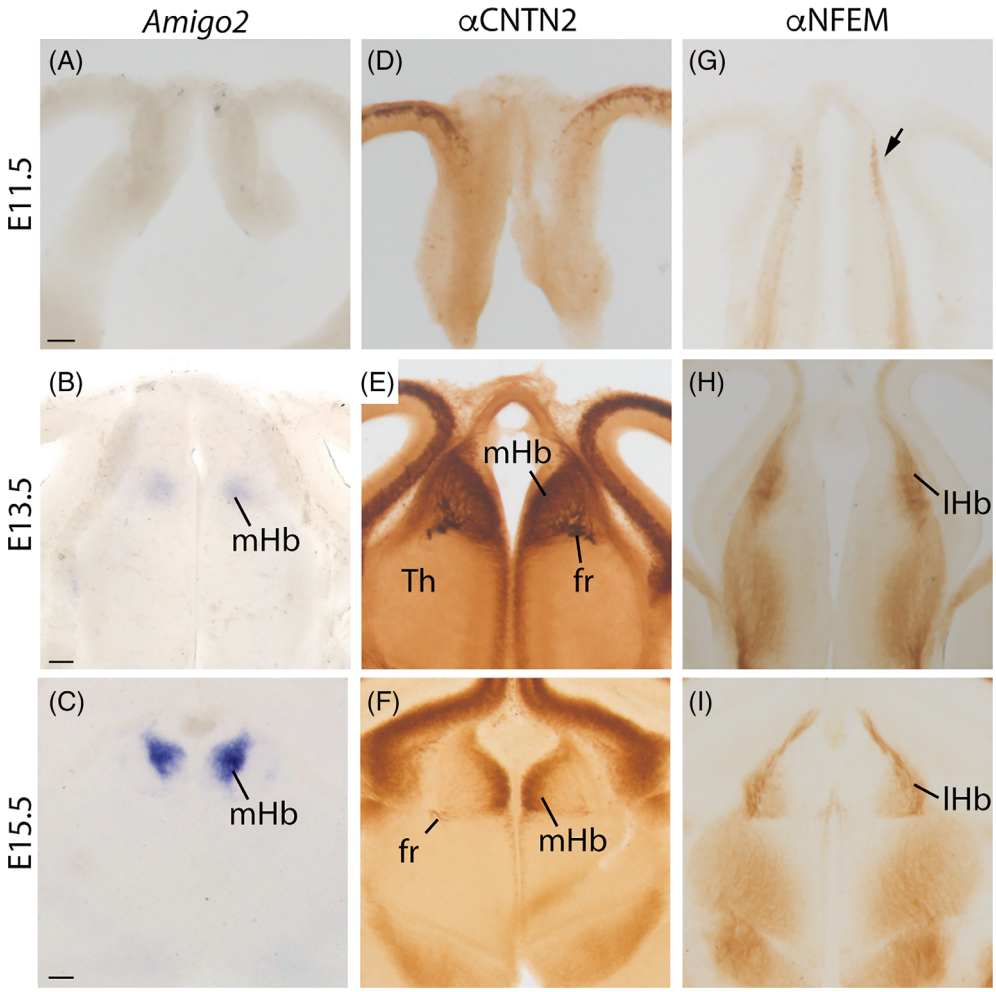

FIGURE 2 *Amigo2* expression in the habenular development. Coronal sections of E11.5 (A, D, G), E13.5 (B, E, H) and E15.5 (C, F, I) brains. *Amigo2* in situ hybridization (A, B, C). Immunohistochemistry against CNTN2 (D, E, F) as mHb marker and NFEM (G, H, I) as lHb marker. The lHb neurons were firstly detected at E11.5 (arrow in G). We were able to follow, at E13.5 and E15.5, the development of both nuclei with the selected markers. fr, fasciculus retroflexus; lHb, lateral habenula; mHb, medial habenula; Th, thalamus. Scale bar: 200 μm

behavior is also accompanied by a segregation of fr axons.[20,41] Labeling mHb axons with *Contactin2* (CNTN2; Figure 1C) and lHb axons with *Neurofilament* (NFEM; Figure 1C), revealed the axonal distribution within the fr (Figure 1D-F). In a sagittal section, we noted how the mHb axons begin to fasciculate tightly in the core of the initial segment of the fascicle, while the lHb axons selectively surround them in the shell of the tract (Figure 1E). This segregation was maintained until the fascicle reached the diencephalic basal plate (Figure 1F). The distribution of mHb axons in the core and lHb axons in the shell of the fr was also displayed in a frontal section (Figure 1D).

2.2 | Amigo2 expression in the developing habenula

Once we confirmed the mHb and lHb axonal organization in the fr, we proceeded to study *Amigo2* expression pattern during embryonic development in comparison with the distribution of CNTN2 and NFEM, well-known markers of the medial and lateral habenular territories, respectively. These markers were used thereafter to describe the phenotypes in our experimental approaches. Habenular *Amigo2* mRNA signal was absent at E11.5 (Figure 2A), but a faint expression was observed in the prospective mHb territory at E13.5 (Figure 2B), and strong mHb expression was present at E15.5 (Figure 2C). We compared this expression with the localization of a specific protein of the mHb (CNTN2) and a specific protein of the lHb (NFEM). CNTN2 was not present at E11.5 (Figure 2D). It displayed broad labeling of the mHb mantle at E13.5 (Figure 2E) and its expression concentrated in the periventricular stratum of the mHb at E15.5 (Figure 2F). On the other hand, NFEM expression was already found at E11.5 in the lHb (Figure 2G), increased at E13.5 (Figure 2H) and covered all the lHb plus the habenular commissure at E15.5 (Figure 2I).

2.3 | Amigo2 loss of function phenotype

With the aim to describe *Amigo2* lack of function in our system, we compared wild type and *Amigo2*$^{-/-}$ E15.5

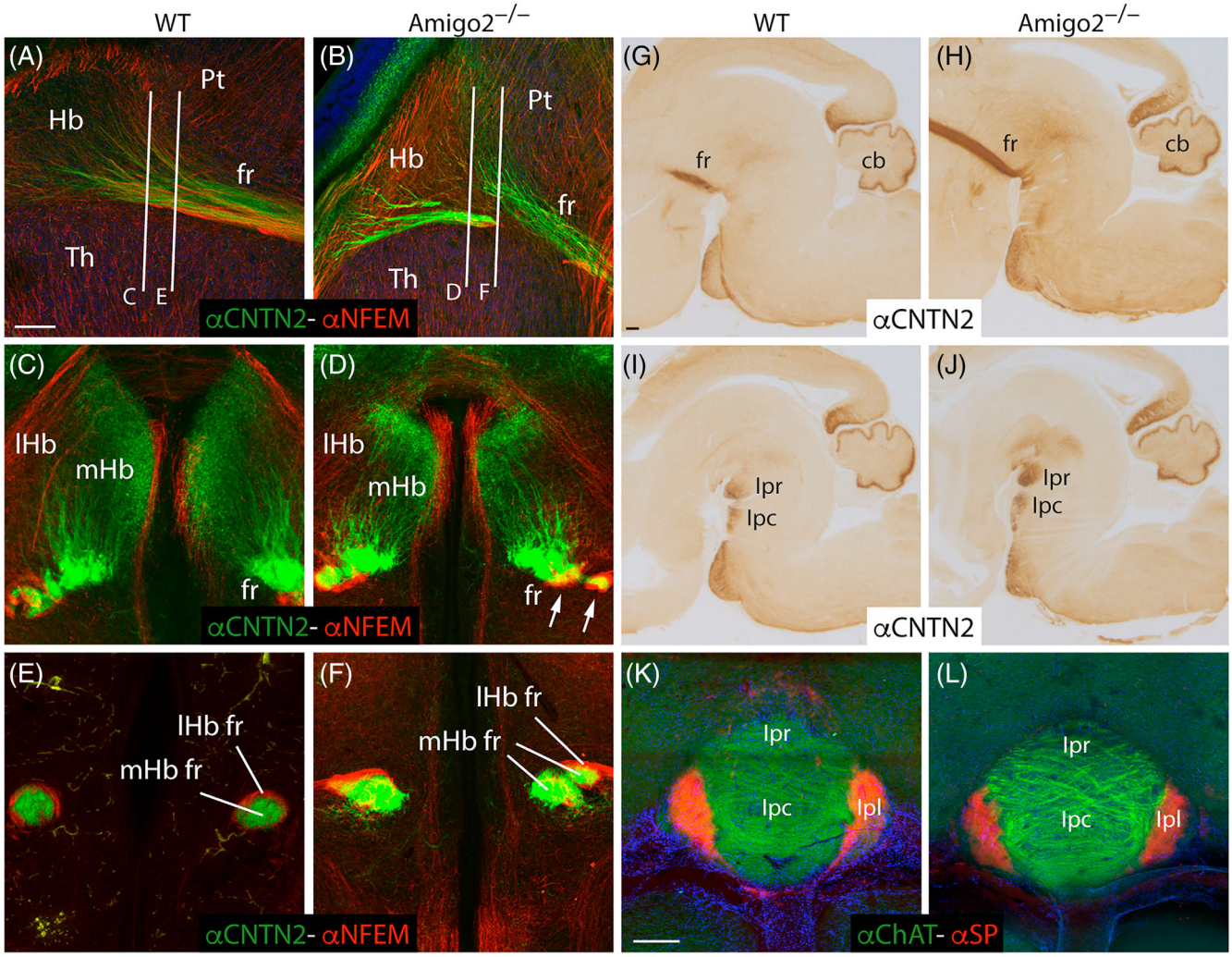

FIGURE 3 Study of the fr phenotype in Amigo2$^{-/-}$ mutant. E15.5 wild type brain sagittal section (A) and E15.5 *Amigo2*$^{-/-}$ brain sagittal section (B). Coronal sections of an E15.5 wild type (C, E) and an E15.5 *Amigo2*$^{-/-}$ mutant brain (D, F). The plane of the coronal sections is indicated with white lines in A and B. All of them are stained with NFEM (as lHb marker) and CNTN2 (as mHb marker). The tract was wide, and even divided in two fascicles in the mutant embryos and the axons were less fasciculated. Sagittal sections of E18.5 wild type (G, I) and *Amigo2*$^{-/-}$ brains (H, J) labeled by immunohistochemistry against CNTN2. In a lateral section, we observed the mHb fr reaching the rhombomere 1 (G) and in a more medial section the two Ip nucleus main components (rostral and caudal) labeled by the innervation of the CNTN2 positive mHb fr axons (I). In the *Amigo2*$^{-/-}$, a wider fr is observed following the expected trajectory (H) and how its fibers innervate with no obvious defect the Ip nucleus (J). Coronal sections of adult wild type (K) and *Amigo2*$^{-/-}$ (L) labeled by immunohistochemistry against ChAT and Substance P. The ventral mHb axons, ChAt positive, innervate the rostral and caudal Ip, while dorsal mHb axons, Substance P positive, innervate the lateral IP subnucleus. No alteration in this innervation was detected in *Amigo2*$^{-/-}$. cb, cerebellum; fr, fasciculus retroflexus; Hb, habenula; Ipc, caudal interpeduncular nucleus; Ipl, lateral interpeduncular nucleus; Ipr, rostral Interpeduncular nucleus; lHb, lateral habenula; lHb fr, lateral habenular axons of the fasciculus retroflexus, mHb, medial habenula; mHb fr, medial habenular axons of the fasciculus retroflexus; Pt, pretectum; SNc, substantia nigra pars compacta; Th, thalamus. Scale bar: 100 μm (A-F) and 200 μm (G-L)

brains. In contrast to wild type conditions, shown in sagittal sections in Figure 3A, mutant brains showed less compact CNTN2-positive mHb axons that occupied a broader territory and delayed their condensation until they reached the ventral superficial portion of the tract; this reveals a failure of fasciculation of this component along the initial dorsoventral course through the alar and basal plates (Figure 3B). In wild type coronal sections of the habenula (white lines in Figure 3A), we detected the mHb axons fasciculating in a single tract as they are surrounded by the lHb axons (Figure 3C, E). In contrast, in mutant coronal sections (white lines in Figure 3B) it was also striking that mHb axons seemed unable to form a normal single compact tract (Figure 3D), and lHb fibers

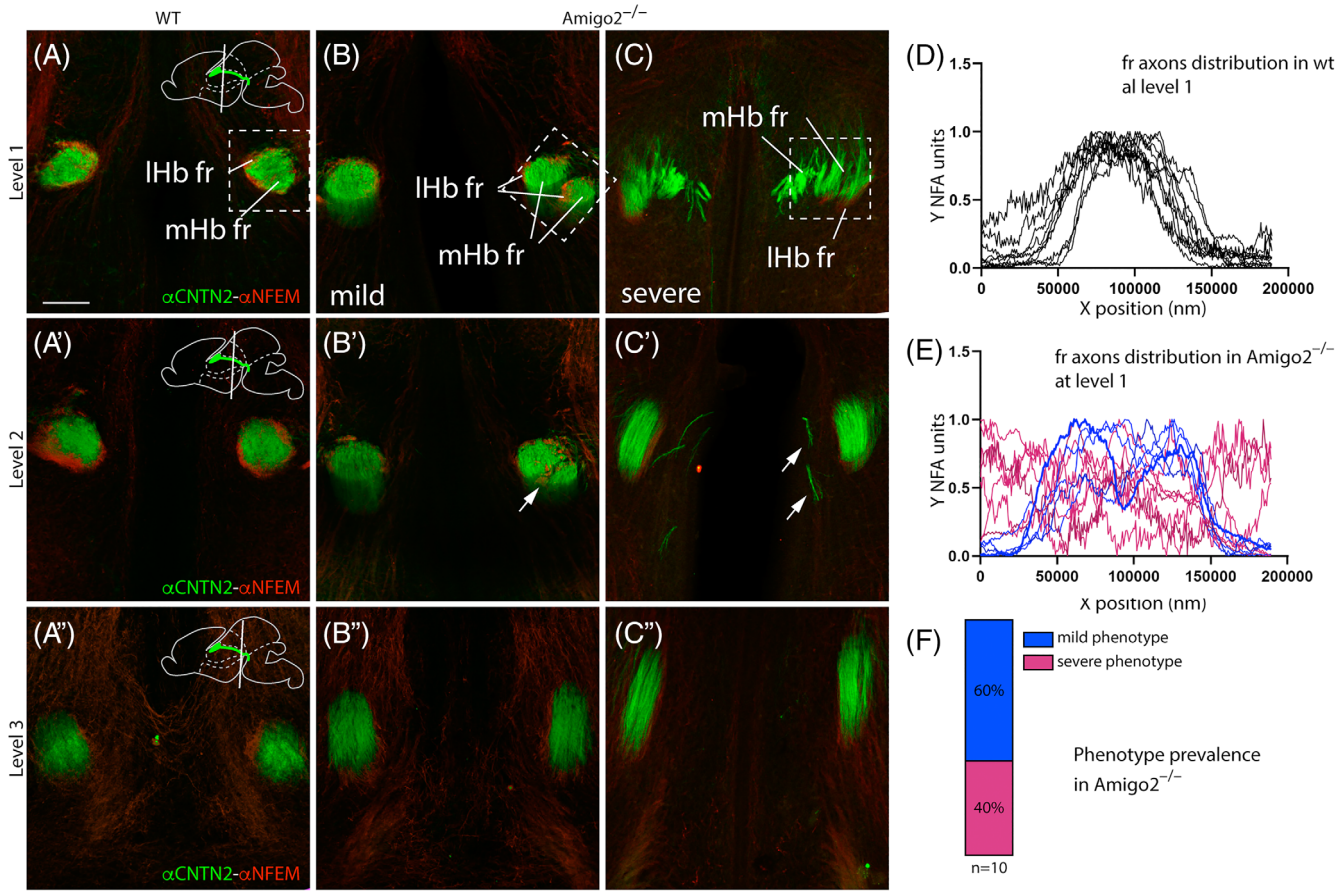

FIGURE 4 Classification of the fr phenotype in *Amigo2*$^{-/-}$ mutant. (A-A″) fr coronal sections at three levels of a E15.5 wild type embryo; (B-B″, C-C″) fr coronal sections at three levels of two E15.5 *Amigo2*$^{-/-}$ mutant embryo, (B) presents a mild phenotype and (C) a severe phenotype. Labeled against CNTN2 (as mHb marker) and NFEM (as lHb marker). The tract was less compacted and generated unilateral aberrant duplications of fr. (D, E) Graphical representation of the normalized arbitrary fluorescent unit distribution of the wild type (D; n = 12) and Amigo2$^{-/-}$ mutant fr with blue for the mild phenotype and magenta for the severe phenotype (E; n = 14). (F) Graphical representation of the phenotype prevalence distribution in Amigo2$^{-/-}$ mutant tracts. To facilitate the reading of the graph we have not included the "normal" side of the mild phenotype. fr, fasciculus retroflexus; lHb fr, lateral habenular axons of the fasciculus retroflexus, mHb fr, medial habenular axons of the fasciculus retroflexus; NFAU; normalized fluorescent arbitrary units. Scale bar: 100 μm

accompanied all disaggregated tract portions generating corresponding shells (arrows in Figure 3D). At the initial portion of the mutant fr, different degrees of fasciculation were observed, even involving left- and right-sided components, with poorly compacted tracts or even with the fibers divided in two distinct fascicles (Figure 3F). This slightly asymmetric phenotype was side independent and inconstant. We also analyzed the trajectory of the fr at E18.5 in the absence of Amigo2. In the wild type, the fr course continues through the paramedian basal midbrain (Figure 3G) to reach the rostral and caudal subnuclei of the Ip formation in the prepontine rostral hindbrain (Figure 3I), In Amigo2$^{-/-}$ specimens, no visible defect was located. The fascicle displays the same route (Figure 3H) reaching its standard target in the hindbrain (Figure 3J). In the adult, Amigo2 expression in the mHb is restricted to its ventral part. We analyzed the localization of choline acetyl transferase (ChAT) and substance P proteins, which are specific markers of ventral and dorsal mHb neurons, respectively. In the wt, ventral mHb axons innervate the central part of the rostral and caudal Ip subnuclei, while dorsal mHb axons innervate the corresponding lateral Ip portions[42] (Figure 3K). The same distribution of ventral and dorsal mHb axons was found in Amigo2$^{-/-}$ specimens (Figure 3L). Therefore, no alteration in the fr guidance mechanism and Ip innervation was detected in the Amigo2 loss-of-function phenotype.

2.4 | Phenotype quantification and variability

Once the loss-of-function phenotype was described, we quantified the alteration observed. We analyzed 12 wild type (Figure 4A-A″) and 14 mutant fr (Figure 4B-B″, C-

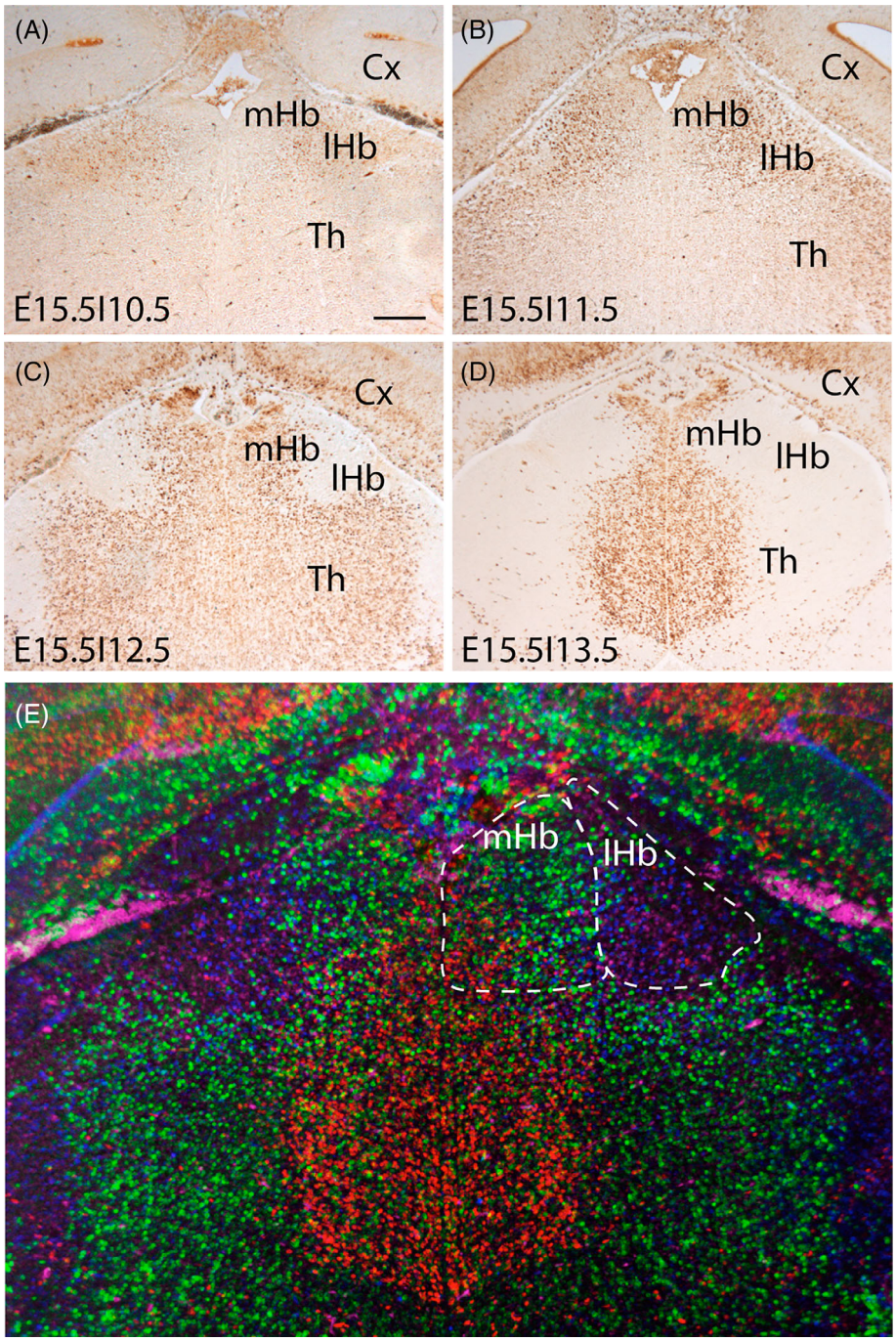

FIGURE 5 Birth-dating of the habenular neurons. Coronal sections of E15.5 wild type brains. The embryos were collected at E15.5 after five BrdU injections during the designated day: 10.5 (A), 11.5 (B), 12.5 (C) and 13.5 (D). In E we show color-coded overlays of the four previous images, by the use of Adobe Photoshop, in order to get a general overview of the habenular birth date, E10.5 in magenta, E11.5 in blue, E12.5 in green and E13.5 in red. The lHb is born around E10.5 and E11.5 meanwhile the mHb is born around E12.5 and E13.5. Cx, cortex; lHb, lateral habenula; mHb, medial habenula; Th, thalamus. Scale bar: 200 μm

C″). This showed in the first place that the mutant phenotype was not constant. In 60% of cases we found a mild phenotype with fr defasciculated unilaterally in two separate tracts (Figure 4B-B″, F), not always in the same side, while in 40% of cases the fr displayed bilateral strong defasciculation (Figure 4C-C″, F).

In order to quantify the distribution of fr fibers, we analyzed three points along the fascicle in wildtype, mild and severe phenotype (level 1 at the initial segment located roughly 100 μm away from the habenula, level 2 at the middle of the dorsoventral course and level 3 at the final dorsoventral position, just before the defasciculation of the lHb axons). The most significant phenotype was found at level 1 in the initial segment. We placed a standard square surface overlay oriented parallel to the largest dimension of the tract complex (one or several partitions), which served to obtain normalized fluorescent arbitrary units measured along the largest dimension of the various separate tract elements the surface of the sectioned tract, representing the results on a cartesian graph. The X axis coincides with the largest dimension of the tract and the Y axis represents the measured

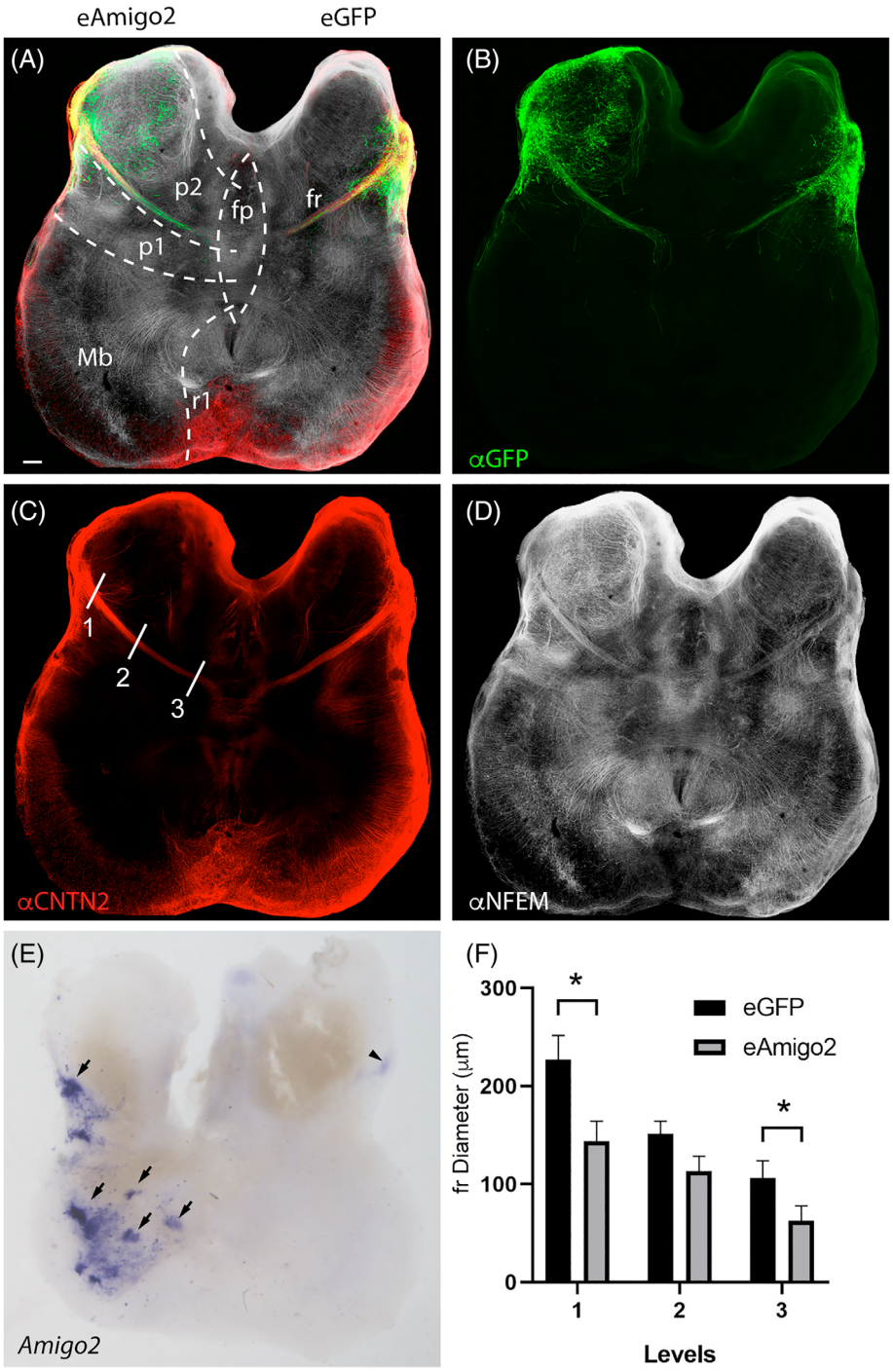

FIGURE 6 Overexpression of Amigo2 in wild type ONTCs. E13,5 wild type ONTCs electroporated with an *Amigo2 + GFP* (left side) and *GFP* (right side) expressing vectors and after 72 h of incubation (A-E). ONTC labeled by immunohistochemistry against GFP (B), CNTN2 (C) and NFEM (D). In the experimental side we labeled the three points of measurement. ONTC labeled by in situ hybridization against *Amigo2*, the arrow indicates ectopic expression in the experimental side, the arrowhead indicates the endogenous expression in the control side (E). Significance was analyzed by Unpaired *t* tests. Significant differences (* < 0.05) among *Amigo2* electroporated and control fr are found at level 1 and 3 (F; n = 4). fp; floorplate; fr; fasciculus retroflexus, Mb, midbrain; p1, prosomere 1 (pretectum); p2, prosomere 2 (thalamus); p3, prosomere 3; r1, rhombomere 1. Scale bar: 200 μm

fluorescent labeling quantity (one or more peaks along the X axis). The distribution in the wild type fr showed a single compact tract with its fibers occupying an average width of 137.11 ± 17.4 μm and a single Gaussian peak of fluorescence distribution (Figure 4D). In contrast, the mutant fr displayed a wider spatial distribution with an average maximum width of 235.5 ± 49.7 μm and a variable number of fluorescence peaks corresponding to the number of defasciculated tracts (mild phenotype in blue and severe phenotype in magenta; Figure 4E). The average tract width was of 210.8 ± 33.3 μm in the mild phenotype and of 272.6 ± 48.4 μm in the severe phenotype. The difference between the wild type and mutant tract width was statistically significant ($P < .0001$ by Unpaired test). Also, the difference between the wild type, mild and severe areal width was statistically significant ($P < .0001$ by One-way ANOVA test). The difference in the distribution of the fr fibers between wild type and mutants was compared by Kolmogorov-Smirnov test and the result was statistically significant ($P < .0001$).

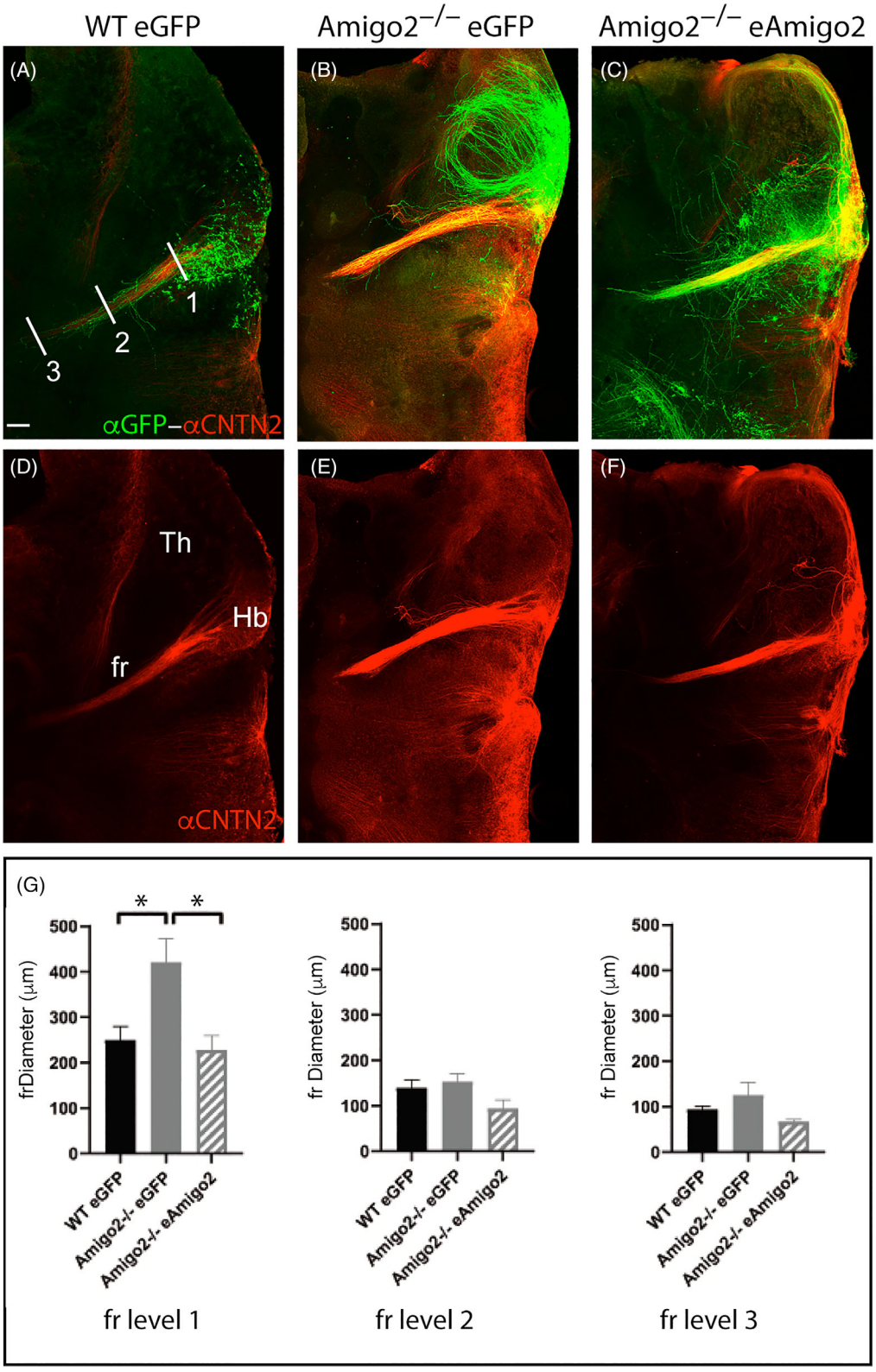

FIGURE 7 *Amigo2*$^{-/-}$ phenotype recovery. E13,5 wild type and mutant ONTCs electroporated with an *Amigo2* + *GFP* or *GFP* expressing vectors and after 72 h of incubation (A-F). Wild-type ONTC *GFP* electroporated (A, D), *Amigo2*$^{-/-}$ *GFP* electroporated (B, E) and *Amigo2*$^{-/-}$ *Amigo2* + *GFP* electroporated (C, F). Labeled against GFP and CNTN2 by immunohistochemistry. The numbers indicated in A indicate the measurement points. Significance was analyzed by One-way ANOVA tests. Significant differences (* < .05) were found among wild type and *Amigo2* electroporated mutant fr at level 1 and also between *Amigo2* electroporated mutant and GFP electroporated mutant fr at level 1 (G). fr, fasciculus retroflexus; Hb, habenula; Th, thalamus. Scale bar: 200 μm

The fasciculation alteration was still visible at level 2 in mild and severe phenotypes when compare with the wild type (arrows in Figure 4A′, B′, C′) but the quantifications of the fr diameters were not statistically significative. At level 3, the fascicle on both phenotypes did not present obvious defects in its fasciculation (Figure 4A″, B″, C″).

2.5 | Amigo2 gain of function

We also studied the effect of *Amigo2* overexpression or gain of function by electroporation of the habenular complex in culture. In order to select the optimal time window correlative with mHb neurogenesis, we analyzed the birth dates of the habenular neurons. The lHb neurons were born between E10.5 and E11.5 while mHb neurons were produced between E12.5 and E13.5 (Figure 5A-E). We selected this last period to target the mHb by electroporation of *Amigo2* functional plasmid vector in Organotypic nervous tissue cultures (ONTCs).

We electroporated *Amigo2* plus *Gfp* expressing plasmid vectors on the left side of the wild-type ONTCs, while *Gfp* was electroporated alone in the right side as a control (n = 4). The electroporated area was easily identified by the presence of GFP fluorescent signal (Figure 6A, B). Moreover, the course of mHb axons was displayed by CNTN2 immunoreaction (Figure 6A, C) and that of the lHb axons by NFEM immunoreaction (Figure 6A, D). The *Amigo2* functional plasmid vector activity was positively tested by in situ hybridization (ISH, Figure 6E). The control side showed the endogenous *Amigo2* expression limited to the habenula (arrowhead in Figure 6E), while the experimental side displayed an expanded electroporated area (arrows in Figure 6E). In order to quantify the phenotype observed, we selected three levels along the fr to measure the tract thickness (close to the origin, at the ventral point of caudalward bending, and at the midpoint between the previous ones; 1-3 in Figure 6B). At the three levels, the electroporated tract diameter was thinner than in the controls. This result was observed not only in the mHb axons (Figure 6C) but also in the lHb axons (Figure 6D). However, the difference was statistically significant only at the upper and lower points ($P < .05$ by Unpaired *t* test in each level; Figure 6F). Thus, an *Amigo2* overexpression in the habenular territory resulted in a thinner fr when compared with the control side.

2.6 | Amigo2$^{-/-}$ phenotype rescue

In order to rescue the phenotype observed in the *Amigo2* mutant we electroporated *Gfp* in wild type (Figure 7A; n = 3) and mutant Hb (Figure 7B; n = 3), as controls, and *Amigo2* plus *Gfp* in mutant Hb (Figure 7C; n = 3). The fr course was shown by CNTN2 labeling and the measure of the tract spread was done at the three levels described above. The *Gfp* electroporated mutant fr displayed a wider spread than the wild type one (Figure 7D, E), while the *Amigo2* electroporated mutant fr was reduced in width compared with the wild-type. However, the observed difference between the samples only was statistically significant at the proximal or initial level ($P < .05$ by One-way ANOVA test in each level, Figure 7G). Functional *Amigo2* is thus able to rescue the phenotype observed in the mutant in terms of the tract diameter.

3 | DISCUSSION

Axonal behavior is regulated by surface molecules that controls the degree of fasciculation processes and the integration of short and long-range signals that guide the growing axons toward their final targets.[17,43,44] The fr is a tightly packed tract originated in the habenular complex. Its fibers are segregated in a core region with axons from the mHb and a shell area with axons from the lHb.[10,11] Evolutionary analysis has suggested that the mammalian mHb is homologous to the primitive habenula of lampreys and teleosts, whereas the lHb would have appeared later in evolution.[45] This sequence may fit with the mammalian fr organization with mHb axons in the core and lHb axons in the shell. All fr axons share the same initial behavior (dorsoventral course across the caudalmost thalamic mantle into the basal plate) but differ in the subsequent tegmental segment. While initially both components follow a fasciculated course, upon arrival at the diencephalic basal domain the lHb axons defasciculate from mHb axons and follow their own terminal course. The fasciculation/defasciculation processes involved in the development of the fr are unknown. Some well-known guidance molecules such as DCC, Robo or Ephrins (among others) generally promote fasciculation.[17] Nevertheless, the specific surface proteins that are involved in the fasciculation of the fr are unknown. By its expression in the mHb at an appropriate time window, *Amigo2* seemed a candidate to play a role in the fasciculation behavior at least of mHb axons.[20]

Our results have shown that *Amigo2* indeed plays a role in the fr fasciculation but not in its navigation, since the fascicle is able to reach normal final targets in absence of the *Amigo2*. The lack of function phenotype results in a variable fr defasciculation (division into two or more separate tracts) that tends to be slightly asymmetric and appears most strongly at the initial segment

of the dorsoventral course. The mammalian Hb, as well as its fr, is a rather symmetric structure in contrast to the reptilian, amphibia and fish counterparts where strong asymmetries have been described.[41,45] Nevertheless, subtle differences have been described also in some rodent strains.[45] The *Amigo2* loss-of-function alteration may uncover subtle heterogeneities existing between both sides (eg, various other interacting molecular determinants), so that the resulting phenotype has different penetrance.

It is safe to assume that a particular sort of axons expresses a cocktail of surface molecules that could have collectively redundant roles in the behavior of the growing fiber. Moreover, the capacity of the different Amigo family members to interact in both homophylic and heterophilic manner may add to the variability in the phenotype (severe vs mild forms) observed after the removal of only one of these surface proteins. Remarkably, the initial defasciculation of mHb axons also produced an alteration in the fasciculation of the lHb axons, which seemed attracted to form shells around the separate packets of mHb axons. This bespeaks of a specific adhesive interaction between the mHb and lHb axons. This result confirms a strong interaction between lHb and mHb axons in the fr.[20,41]

Finally, *Amigo2* electroporation reduced the fr width in the wild type and partly rescued in the mutant the altered phenotype observed without reaching the full wild type level. The fact that the recovery was consistent and that control and experimental ONTCs sides shared the same electroporation conditions suggested us that cell death or ectopic effects were not interfering in our overexpression experiments. Thus, *Amigo2* is a molecular determinant to define the fasciculation level of the fr and our results allowed us to postulate that *Amigo2* is involved in the fasciculation of the fr particularly at the start of its descending course (it does not seem to have a similar role along the final descending route of the tract into the hindbrain) but does not intervene in navigational guidance proper.

4 | EXPERIMENTAL PROCEDURES

4.1 | Mouse strains

For staging, the day when the vaginal plug was detected was considered as embryonic day 0.5 (E0.5). All mouse manipulation and experimental procedures were performed according to the directives of the Spanish and European Union governments and the protocols were approved by the Universidad Miguel Hernández OIR Committee (2016/VSC/PEA/00190). The *Amigo2* knockout line generation and genotype was previously described in Li et al.[46]

4.2 | In situ hybridization and immunohistochemistry

Mouse embryo brains were fixed overnight in 4% paraformaldehyde (PFA) in phosphate buffered saline (PBS). Samples were agarose-embedded and sectioned at 100 μm by vibratome.

For ISH, the tissue was post fixed in 4% PFA. Next, it was rinsed in PBS, and pre-hybridized with hybridization buffer (deionized formamide [Ambion 50%], sodium citrate salt [SSC ×5, pH 5.3], heparin [Sigma-Aldrich 50 lg/ml], Tween 20 [Sigma-Aldrich, 0.1%]). The digoxigenin-labeled RNA probe (*Amigo2*, BC095990) was denaturalized at 80°C. The tissue was incubated in hybridization buffer with the probe over night at 65°C. The samples were washed (SSC ×2 pH 4.5, formamide 50% and SDS 1%, water 50%) five times at 65°C. Afterwards, the samples were washed with MABT ×1 (NaCl (150 mM), maleic acid (100 mM, Sigma-Aldrich) NaOH (Sigma-Aldrich) to obtain pH 7.5, and Tween 20 0.1%) and the tissue was blocked in sheep serum 20%, (Sigma-Aldrich, #S3772) and 2% of blocking reagent (Roche; #11096176001) in MABT ×1 and was incubated overnight with an alkaline phosphatase-coupled anti-digoxigenin antibody (Roche Diagnostics, #1109327 4910). Next day, the samples were extensively washed with MABT ×1 to remove the traces of non-specific bound antibodies. Before the colorimetric reaction, the samples were incubated in NTMT (NaCl [0.1 M], Tris-HCl [0.2 M, pH 9.5], MgCl2 [0.05 M] and Tween 20 [0.1%]). Standard NBT/BCIP (Boehringer, Mannheim) was used as a chromogenic substrate to detect the probes. The alkaline phosphatase reacts with this substrate producing a solid precipitate.

For IHC, it was performed as previously described.[47] The primary antibodies used were: αBrdU (1:200; M 0744/Dako), αChAT (1:150; AB144P/Chemicon), αCNTN2 (1:500; AF4439/RD Systems), αDCC (1:100; #sc-6535/Santa Cruz), αNFEM (1:1000; AB1987/Chemicon), αROBO3 (1:300; AF3076/Rdsystems), αSubstance P (1:200; MAB356/Millipore) and αTH (1:1000; AB152/Sigma-Aldrich).

4.3 | Axonal tracing

For axonal tracing, the embryonic brains were fixed for 1 h in 4% PFA. Small Dil crystals (1,1′-dioctadecyl 3,3,3′,3′-tetramethylindocarbo-cyanine perchlorate;

Molecular Probes) were inserted into the habenular nuclei. The labeled brains were incubated at 37°C in 4% PFA until the tracers had diffused sufficiently. The brains were sectioned and IHC processed without detergent to avoid the DiI signal loss.

4.4 | Birth dating by BrdU labeling

For detection of the peak of neurogenic proliferation, BrdU was administered intraperitoneally to the pregnant females (3 mg/100 g body weight) every 2 h, for a period of 10 h (five injections in total) starting at desired stages. The embryos were extracted at E15.5.

4.5 | Organotypic nervous tissue culture

They were developed as previously described (Moreno-Bravo et al).[12] In brief, E13.5 embryos neural tubes were dissected and opened along the dorsal midline and telencephalic vesicles and hypothalamus regions were removed. The diencephalic fr developing area was kept intact. Finally, the dissected explants were cultured like an open book with the ventricular surface looking upwards on a polycarbonate membrane (Whatman Nuclepore Track-Etched Membranes). The ONTCs in the incubator 3 h at 37°C, 5% CO2 until the electroporation process.

4.6 | Overexpression of Amigo2 in ONTCs experiment

Amigo2 (BC095990) and/or PCX-GFP expressing vectors were electroporated focally in ONTCs. For the electroporation procedure the ONTCs and its supporting membrane was placed onto an 1% agarose block within a setup of two horizontally oriented platinum electrodes. An 1% agarose column was attached to the mobile upper electrode. Two electric pulses of 80 V and 5 ms, spaced 500 ms were applied using a square pulse electroporator. The electroporated ONTCs were incubated 72 h at 37°C, 5% CO_2 in enriched DMEM.

4.7 | ONTCs immunochemistry

The incubated ONTCs were fixed in 4% PFA for 3 h. After dehydration in methanol, the samples were bleached using 6% Hydrogen Peroxide solution in 100% methanol O/N at 4°C. Samples were blocked using PBS-GT, PBS containing 0,2% Gelatin (Prolabo) and 0.5% Triton X-100 (Sigma-Aldrich) O/N at RT and then incubated in agitation for 7 days at 37°C with αCNTN2 (1:500; AF4439/RD Systems), αNFEM (1:1000; AB7794/Abcam), αGFP (1500: GFP-1020/AVES). This was followed by six washes of 30 min in PBS-GT 0.5% at RT and incubated with the secondary antibodies O/N at 37°C. ONTCs were counterstained with DAPI diluted in PBS at 0,001% and incubated 10 min. at room temperature.

4.8 | Image processing and quantification

Bright field and fluorescent images were acquired with a camera (Leica DFC500) associated with a stereomicroscope (Leica Fluo-III) and with Leica Confocal SPEII, respectively. The figures were composed with Adobe System software. The axon trajectory in the *Amigo2* mutant and control sections was quantified at three levels. Level 1 was at the proximal segment of the fr (100 μm from the Hb), level 3 was before the caudal bending point of the fascicle and level 2 at the mid position between the other two. We quantified by the distribution of red and green fluorophores ligated to the two sorts of studied axons in the fr area by the Plot Profile tool of the Fiji software in normalized photographs to avoid background fluorescence interference. The fr phenotype in *Amigo2* mutant, control and electroporated ONTCs was quantified at three fixed levels along the longitudinal aspect of the fascicle by Fiji software. The statistical analysis was performed with Kolmogorov-Smirnov test (Figure 4), Unpaired *t* tests (Figures 4 and 6) and One-way ANOVA test (Figures 4 and 7) using GraphPad Prism software. All authors consent to participate and publish the data included in this manuscript.

AUTHOR CONTRIBUTIONS

Verónica Company: Conceptualization (equal); data curation (equal); formal analysis (equal); investigation (equal); methodology (equal); validation (equal); visualization (equal); writing – original draft (equal). **Raquel Murcia-Ramón:** Investigation (equal); methodology (equal). **Abraham Andreu-Cervera:** Investigation (equal); methodology (equal). **Paula Aracil-Pastor:** Data curation (supporting); formal analysis (supporting); investigation (supporting). **Francisca Almagro-García:** Investigation (supporting); methodology (supporting). **Salvador Martínez:** Conceptualization (lead); funding acquisition (lead); resources (lead); writing – original draft (lead). **Diego Echevarría:** Conceptualization (equal); funding acquisition (lead); investigation (equal); methodology (equal); resources (equal); supervision (equal); validation (equal); writing – original draft

(equal). **Eduardo Puelles:** Conceptualization (lead); data curation (lead); formal analysis (lead); funding acquisition (lead); investigation (lead); methodology (lead); resources (lead); supervision (lead); validation (lead); visualization (lead); writing – original draft (lead); writing – review and editing (lead).

ACKNOWLEDGMENTS

Work supported by MINECO/AEI/FEDER (BFU2013-48230) to Eduardo Puelles and Diego Echevarría; MINECO/AEI/FEDER (SAF2017-83702-R), GVA (PROMETEO/2018/041), ISCIII ("RD16/001/0010"), co-funded by ERDF/ESF, "Investing in your future", and FTPGB (FTPGB18/SM) to Salvador Martínez; MECD (FPU16/03853) to Verónica Company. The Institute of Neurosciences is a "Centre of Excellence Severo Ochoa." We thank Dr. H. Rauvala for sharing Amigo2$^{-/-}$ strain.

CONFLICT OF INTEREST

The authors declare that the research was conducted in the absence of any commercial or financial relationships that could be construed as a potential conflict of interest.

DATA AVAILABILITY STATEMENT

The data that support the findings of this study are available from the corresponding author upon reasonable request.

ETHICS STATEMENT

All mouse experiments were performed according to protocols approved by the Universidad Miguel Hernandez OEP committee (2016/VSC/PEA/00190).

ORCID

Eduardo Puelles https://orcid.org/0000-0002-0560-9240

REFERENCES

1. Nieuwenhuys R, Voogd J, van Huijzen C. Greater limbic system. *The Human Central Nervous System*. 4th ed. Springer Verlag: Berlin Heidelberg; 2008:917-941.
2. Nikolenko VN, Oganesyan MV, Rizaeva NA, et al. Amygdala: neuroanatomical and morphophysiological features in terms of neurological and neurodegenerative diseases. *Brain Sci*. 2020; 10(8):1-18. doi:10.3390/brainsci10080502
3. Duman RS, Sanacora G, Krystal JH. Altered connectivity in depression: GABA and glutamate neurotransmitter deficits and reversal by novel treatments. *Neuron*. 2019;102(1):75-90. doi:10.1016/j.neuron.2019.03.013
4. Hu H, Cui Y, Yang Y. Circuits and functions of the lateral habenula in health and in disease. *Nat Rev Neurosci*. 2020; 21(5):277-295. doi:10.1038/s41583-020-0292-4
5. Aizawa H, Amo R, Okamoto H. Phylogeny and ontogeny of the habenular structure. *Front Neurosci*. 2011;5:1-7. doi:10.3389/fnins.2011.00138
6. Bühler A, Carl M. Zebrafish tools for deciphering habenular network-linked mental disorders. *Biomolecules*. 2021;11(2):1-18. doi:10.3390/biom11020324
7. Fakhoury M. The habenula in psychiatric disorders: more than three decades of translational investigation. *Neurosci Biobehav Rev*. 2017;83:721-735. doi:10.1016/j.neubiorev.2017.02.010
8. Fakhoury M. The dorsal diencephalic conduction system in reward processing: spotlight on the anatomy and functions of the habenular complex. *Behav Brain Res*. 2018;348:115-126. doi:10.1016/j.bbr.2018.04.018
9. Roman E, Weininger J, Lim B, et al. Untangling the dorsal diencephalic conduction system: a review of structure and function of the stria medullaris, habenula and fasciculus retroflexus. *Brain Struct Funct*. 2020;225(5):1437-1458. doi:10.1007/s00429-020-02069-8
10. Ichijo H, Toyama T. Axons from the medial habenular nucleus are topographically sorted in the fasciculus retroflexus. *Anat Sci Int*. 2015;90(4):229-234. doi:10.1007/s12565-014-0252-z
11. Herkenham M, Nauta WJH. Efferent connections of the habenular nuclei in the rat. *J Comp Neurol*. 1979;187(1):19-47. doi:10.1002/cne.901870103
12. Moreno-Bravo JA, Martinez-Lopez JE, Madrigal MP, et al. Developmental guidance of the retroflex tract at its bending point involves Robo1-Slit2-mediated floor plate repulsion. *Brain Struct Funct*. 2016;221(1):665-678. doi:10.1007/s00429-014-0932-4
13. Company V, Andreu-Cervera A, Madrigal MP, et al. Netrin 1-mediated role of the substantia Nigra pars compacta and ventral tegmental area in the guidance of the medial Habenular axons. *Front Cell Dev Biol*. 2021;9:1183. doi:10.3389/fcell.2021.682067
14. Funato H, Saito-Nakazato Y, Takahashi H. Axonal growth from the habenular nucleus along the neuromere boundary region of the diencephalon is regulated semaphorin 3F and netrin-1. *Mol Cell Neurosci*. 2000;16(3):206-220. doi:10.1006/mcne.2000.0870
15. Sahay A, Molliver ME, Ginty DD, Kolodkin AL. Semaphorin 3F is critical for development of limbic system circuitry and is required in neurons for selective CNS axon guidance events. *J Neurosci*. 2003;23(17):6671-6680. doi:10.1523/jneurosci.23-17-06671.2003
16. Kantor DB, Chivatakarn O, Peer KL, et al. Semaphorin 5A is a bifunctional axon guidance cue regulated by heparan and chondroitin sulfate proteoglycans. *Neuron*. 2004;44(6):961-975. doi:10.1016/j.neuron.2004.12.002
17. Spead O, Poulain FE. Trans-axonal signaling in neural circuit wiring. *Int J Mol Sci*. 2020;21(14):1-19. doi:10.3390/ijms21145170
18. Petrovic M, Schmucker D. Axonal wiring in neural development: target-independent mechanisms help to establish precision and complexity. *Bioessays*. 2015;37(9):996-1004. doi:10.1002/BIES.201400222
19. Wang L, Marquardt T. What axons tell each other: axon–axon signaling in nerve and circuit assembly. *Curr Opin Neurobiol*. 2013;23(6):974-982. doi:10.1016/J.CONB.2013.08.004
20. Schmidt ERE, Brignani S, Adolfs Y, et al. Subdomain-mediated axon-axon signaling and chemoattraction cooperate to regulate afferent innervation of the lateral habenula. *Neuron*. 2014; 83(2):372-387. doi:10.1016/j.neuron.2014.05.036

21. Giger RJ, Cloutier JF, Sahay A, et al. Neuropilin-2 is required in vivo for selective axon guidance responses to secreted semaphorins. *Neuron*. 2000;25(1):29-41. doi:10.1016/S0896-6273(00)80869-7
22. Worzfeld T, Puschel AW, Offermanns S, Kuner R. Plexin-B family members demonstrate non-redundant expression patterns in the developing mouse nervous system: an anatomical basis for morphogenetic effects of Sema4D during development. *Eur J Neurosci*. 2004;19(10):2622-2632. doi:10.1111/j.0953-816X.2004.03401.x
23. Perälä NM, Immonen T, Sariola H. The expression of plexins during mouse embryogenesis. *Gene Expr Patterns*. 2005;5(3):355-362. doi:10.1016/j.modgep.2004.10.001
24. Laeremans A, Nys J, Luyten W, D'Hooge R, Paulussen M, Arckens L. AMIGO2 mRNA expression in hippocampal CA2 and CA3a. *Brain Struct Funct*. 2013;218(1):123-130. doi:10.1007/s00429-012-0387-4
25. Park H, Lee S, Shrestha P, et al. AMI GO2, a novel membrane anchor of PDK1, controls cell survival and angiogenesis via Akt activation. *J Cell Biol*. 2015;211(3):619-637. doi:10.1083/jcb.201503113
26. Kuja-Panula J, Kiiltomäki M, Yamashiro T, Rouhiainen A, Rauvala H. AMIGO, a transmembrane protein implicated in axon tract development, defines a novel protein family with leucine-rich repeats. *J Cell Biol*. 2003;160(6):963-973. doi:10.1083/jcb.200209074
27. Ono T, Sekino-Suzuki N, Kikkawa Y, Yonekawa H, Kawashima S. Alivin 1, a novel neuronal activity-dependent gene, inhibits apoptosis and promotes survival of cerebellar granule neurons. *J Neurosci*. 2003;23(13):5887-5896. doi:10.1523/jneurosci.23-13-05887.2003
28. Wagner F, Stroh T, Veh RW. Correlating habenular subnuclei in rat and mouse by using topographic, morphological, and cytochemical criteria. *J Comp Neurol*. 2014;522(11):2650-2662. doi:10.1002/cne.23554
29. Zhao X, Kuja-Panula J, Sundvik M, et al. Amigo adhesion protein regulates development of neural circuits in zebrafish brain. *J Biol Chem*. 2014;289(29):19958-19975. doi:10.1074/jbc.M113.545582
30. Miyake N, Tonoki H, Gallego M, et al. Phenotype-genotype correlation in two patients with 12q proximal deletion. *J Hum Genet*. 2004;49(5):282-284. doi:10.1007/s10038-004-0144-5
31. Gimelli S, Makrythanasis P, Stouder C, Antonarakis SE, Bottani A, Béna F. A de novo 12q13.11 microdeletion in a patient with severe mental retardation, cleft palate, and high myopia. *Eur J Med Genet*. 2011;54(1):94-96. doi:10.1016/j.ejmg.2010.09.008
32. Rengasamy Venugopalan S, Farrow E, Sanchez-Lara PA, et al. A novel nonsense substitution identified in the AMIGO2 gene in an Occulo-Auriculo-vertebral spectrum patient. *Orthod Craniofacial Res*. 2019;22(S1):163-167. doi:10.1111/ocr.12259
33. Guida V, Calzari L, Fadda MT, et al. Genome-wide DNA methylation analysis of a cohort of 41 patients affected by oculo-auriculo-vertebral Spectrum (OAVS). *Int J Mol Sci*. 2021;22(3):1-19. doi:10.3390/ijms22031190
34. Fontanals-Cirera B, Hasson D, Vardabasso C, et al. Harnessing BET inhibitor sensitivity reveals AMIGO2 as a melanoma survival gene. *Mol Cell*. 2017;68(4):731-744.e9. doi:10.1016/j.molcel.2017.11.004
35. Huo T, Canepa R, Sura A, Modave F, Gong Y. Colorectal cancer stages transcriptome analysis. *PLoS One*. 2017;12(11):1-11. doi:10.1371/journal.pone.0188697
36. Kanda Y, Osaki M, Onuma K, et al. Amigo2-upregulation in tumour cells facilitates their attachment to liver endothelial cells resulting in liver metastases. *Sci Rep*. 2017;7:1-13. doi:10.1038/srep43567
37. Sonzogni O, Haynes J, Seifried LA, et al. Reporters to mark and eliminate basal or luminal epithelial cells in culture and in vivo. *PLoS Biol*. 2018;16(6):e2004049. doi:10.1371/journal.pbio.2004049
38. Nakamura S, Kanda M, Shimizu D, et al. AMIGO2 expression as a potential prognostic biomarker for gastric cancer. *Anticancer Res*. 2020;40(12):6713-6721. doi:10.21873/anticanres.14694
39. Liu Y, Yang J, Shi Z, et al. In vivo selection of highly metastatic human ovarian cancer sublines reveals role for AMIGO2 in intra-peritoneal metastatic regulation. *Cancer Lett*. 2021;503:163-173. doi:10.1016/j.canlet.2021.01.024
40. Braisted JE, Catalano SM, Stimac R, et al. Netrin-1 promotes thalamic axon growth and is required for proper development of the thalamocortical projection. *J Neurosci*. 2000;20(15):5792-5801. doi:10.1523/jneurosci.20-15-05792.2000
41. Bianco IH, Wilson SW. The habenular nuclei: a conserved asymmetric relay station in the vertebrate brain. *Philos Trans R Soc B Biol Sci*. 2009;364(1519):1005-1020. doi:10.1098/rstb.2008.0213
42. Quina LA, Harris J, Zeng H, Turner EE. Specific connections of the interpeduncular subnuclei reveal distinct components of the habenulopeduncular pathway. *J Comp Neurol*. 2017;525(12):2632-2656. doi:10.1002/CNE.24221
43. Chédotal A, Richards LJ. Wiring the brain: the biology of neuronal guidance. *Cold Spring Harb Perspect Biol*. 2010;2(6):1-17. doi:10.1101/cshperspect.a001917
44. Kolodkin AL, Tessier-Lavigne M. Mechanisms and molecules of neuronal wiring: a primer. *Cold Spring Harb Perspect Biol*. 2011;3(6):1-14. doi:10.1101/cshperspect.a001727
45. Concha ML, Wilson SW. Asymmetry in the epithalamus of vertebrates. *J Anat*. 2001;199(1–2):63-84. doi:10.1046/j.1469-7580.2001.19910063.x
46. Li Z, Khan MM, Kuja-Panula J, et al. AMIGO2 modulates T cell functions and its deficiency in mice ameliorates experimental autoimmune encephalomyelitis. *Brain Behav Immun*. 2017;62:110-123. doi:10.1016/j.bbi.2017.01.009
47. Murcia-Ramón R, Company V, Juárez-Leal I, et al. Neuronal tangential migration from Nkx2.1-positive hypothalamus. *Brain Struct Funct*. 2020;225(9):2857-2869. doi:10.1007/s00429-020-02163-x

How to cite this article: Company V, Murcia-Ramón R, Andreu-Cervera A, et al. Adhesion molecule *Amigo2* is involved in the fasciculation process of the fasciculus retroflexus. *Developmental Dynamics*. 2022;251(11):1834-1847. doi:10.1002/dvdy.513